JOURNAL OF PROPULSION AND POWER
Vol. 22, No. 1, January–February 2006

Morphological Characterization and Particle Sizing of Alumina Particles in Solid Rocket Motor

S. Gossé* and L. Hespel†
ONERA-DOTA, 31055 Toulouse CEDEX 04, France
P. Gossart‡
ONERA-DOTA, 91761 Palaiseau CEDEX, France
and
A. Delfour§
ONERA-DOTA, 31055 Toulouse CEDEX 04, France

Rocket propulsion by solid aluminized propellants produces large amounts of alumina particles, which are the main cause of the plume's radiative properties. There are two major factors to consider when assessing the plume's radiative properties using simulation tools. One is the optical properties of Al_2O_3 particles and the other, their size distribution. As the morphology and nature (e.g., phase) of the particles directly impact on their optical properties and indirectly on particle size measurement, physicochemical analyses are a useful way of evaluating these two relevant parameters. We conducted shots experiments on a subscale solid rocket motor. Two experimental setups were used to characterize the particles for each shot: an in situ Mie light-scattering granulometer and an impact/collection system. We also conducted several physicochemical analyses on the collected particles. This paper is mainly focused on the main results of particle size and morphology characterization, whereas the physicochemical results would be presented in a next paper. We especially discuss the presence of hollow spherical particles revealed by scanning electron microscopy and transmission electron microscopy, and we tentatively try to explain this phenomenon and its impact on in situ particle sizing.

Nomenclature

C	=	extinction, scattering and absorption cross sections, μm^2
C^*	=	steam water concentration, mol/m^3
D_{32}	=	Sauter mean diameter of the particle size distribution, μm
$dC_s/d\Omega$	=	differential scattering cross section
$f(R)$	=	particle size distribution defined by number, μm^{-4}
K	=	extinction, scattering, and absorption coefficients, μm^{-1}
$m(\lambda)$	=	complex relative spectral optical index (relative to the surrounding medium)
P_e	=	external pressure, Pa
$P_{H_2O}^{steam}$	=	partial pressure of steam water, atm
P_i	=	internal pressure, Pa
R	=	mantle radius of the sphere, μm
R_c	=	core radius of the sphere, μm
S_w	=	specific surface area, m^2/g
T	=	temperature, K
t	=	transmittance
$V(R)$	=	particle size distribution defined by volume, μm^{-1}
$\Delta V(\theta)$	=	observed volume for the scattering angle θ
$\Delta\theta(\theta)$	=	angular aperture for the scattering angle θ, deg
$\Delta\Omega(\theta)$	=	collection solid angle for the scattering angle θ, sr
θ	=	scattering angle, deg
λ	=	wavelength, μm
$\rho_{al_2o_3}^{s,l}$	=	solid and liquid density of alumina, g/cm^3
$\bar{\rho}$	=	mean particle density, g/cm^3
σ	=	surface tension, N/m
υ	=	steam water solubility (mg H_2O/g Al_2O_3) contributing to spitting phenomenon
υ_S	=	saturated steam water solubility (mg H_2O/g Al_2O_3) contributing to spitting phenomenon
υ_T	=	total steam water solubility (mg H_2O/g Al_2O_3)
ϖ	=	wave number, cm^{-1}

Received 24 September 2004; revision received 3 June 2005; accepted for publication 8 June 2005.

*Ph.D. Student, 02, av. E. Belin.
†Head, Research Unit, 02, av. E. Belin; laurent.hespel@onecert.fr.
‡Postdoctoral Fellow, Chemin de la Hunière.
§Research Engineer, 02, av. E. Belin.

Introduction

AN ongoing project is designed to improve knowledge of the infrared (IR) and ultraviolet (UV) signatures of rocket plumes. Substantial efforts have been made to model all of the aerothermochemical effects[1] and radiative transfer.[2] To compare the measured radiative properties with the numerical simulations, shots experiments were performed on a subscale solid rocket motor (SRM). Various experimental setups were used to characterize the plume and estimate the IR and UV signatures.[3] A SRM with aluminized propellants produces large amounts of alumina particles that mainly contribute to plume signatures. Consequently, the radiative properties of the cloud of alumina particles in the rocket exhaust have become the subject of increasing interest over the past few years.[4–6] We therefore focus on the determination of the optical properties[7] (e.g., refractive index) and physical properties[7,8] (e.g., particle size) of alumina particles in SRM plumes. Preliminary papers[9,10] have been already presented to introduce the partial results obtained from few experiments carried out during the year 2002. New experiments conducted during 2003 were successful for the capture of grams of exhausted alumina. Therefore, new techniques, which are reported here, were applied to the characterization of the collected powders. Because these results modify some of our previous conclusions, we resume the preceding works in this full paper under a new lighting.

Alumina particles were characterized during the shots experiments by an instrument for in situ particle sizing and a particle collection system. Optical techniques are well-established methods of providing high quality results for in situ measurements and are therefore particularly suitable for particle sizing in SRM exhausts.[11–13] A Mie light-scattering granulometer[14,15] was developed in order

to determine the particle size distribution (PSD) from direct measurements of laser light single scattering during shots experiments. Two distinct setups were also used to collect alumina fumes: an impact system and a cyclone collection system. The collected or impacted particles were analyzed by scanning electron microscopy (SEM), transmission electron microscopy (TEM), and the Brunauer, Emmet, Teller (BET) Method. As the nonporosity of particles was confirmed by the BET analyses, density measurements of the collected powder were performed with a helium pycnometer. The measured mean density (typically 3.5 g/cm^3) of the collected particles is slightly lower than the bulk alumina density. Low densities in the 2.5 ± 1 g/cm^3 range have already been observed in collected alumina particles. It was most often explained by assuming that the exhaust particles were highly porous,[16] even if the presence of hollow particles were not excluded.[5,17] In this work, SEM and TEM observations of collected/impacted samples clearly revealed the presence of hollow particles, even if this phenomenon concerns only few percents of the collected particles.

The possible presence of inhomogeneous particles in the plume could induce errors in the estimation of the particle cloud's radiative properties. First, heterogeneity directly influences the assessment of radiative parameters. The second effect is indirect and related to the predominant contribution of PSD in the estimation of the cloud's radiative properties. As PSD is obtained through an inverse method based on a model predicting the scattering properties of a sphere, the impact of this heterogeneity on the determination of PSD must be considered. In both cases, a better comprehension of phenomena deriving heterogeneity is required. The melted ceramics (e.g., volcano lava) or metals (e.g., in welding process) can absorb large amount of gas. Because of its higher density, the solid state cannot contain as much gas as the liquid form. The surplus of gas is then expulsed during solidification. This phenomenon is denoted fluxing or spitting. The high solubility of water steam in liquid alumina[18] associated to a partial steam water vapor pressure inside the combustion chamber about 5 atm could both be sufficient to induce the spitting phenomenon for alumina particles. Considering spitting phenomenon with few assumptions, we proposed an empirical model to predict the heterogeneity comportment. We then adjusted this model to obtain heterogeneity laws matching the SEM–TEM experimental data.

The inverse method associated with the Mie light-scattering granulometer was then modified to include a heterogeneity law. The measured light-scattering diagrams are inverted with both assumptions of homogeneous and heterogeneous spheres. The size distribution and the physicochemical properties of the collected particles can be influenced by their path and thermal history in the plume. To compare the in situ PSD to the collected one, spectral extinction measurements were performed using several potassium bromide (KBr) pellets containing collected particles. The inverse method initially designed for Mie scattering data was adapted to spectral extinction data. As most of the collected particles are homogeneous, the PSD of collected particles is derived only considering full spheres. Because of the possible selectivity of the cyclone in particle collecting and the probable presence of aggregates in the collected particles, few biases can nevertheless exist and should be considered.

Finally, using all of the retrieved PSD, we derived the mean density, the mean diameter, and the mass fraction of γ-Al_2O_3. These data were then compared with the same parameters directly derived from physicochemical analyses of the collected particles (see Refs. 7 and 8 for more details). Considering all of these results, the accuracy of the determined PSD and the pertinence of the heterogeneity law are then evaluated and discussed.

Shots Experiments on a Subscale SRM

General Description of the Shots Experiments

Figure 1 is a schematic diagram of the test bench used for the shots experiments, showing the layout of the various measuring instruments. Spectral measurements of the plume were carried out using an IR spectrophotometer and UV and IR cameras. As we are focusing on particle characterization, we do not discuss these experimental setups and their associated results. In the following, we describe more precisely the instrumentation used for in situ particle sizing, that is, a light-scattering nephelometer and the tools developed to collect the particles.

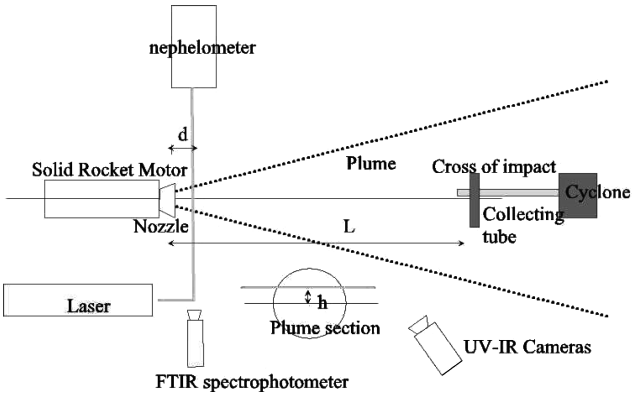

Fig. 1 Schematic representation of the test bench.

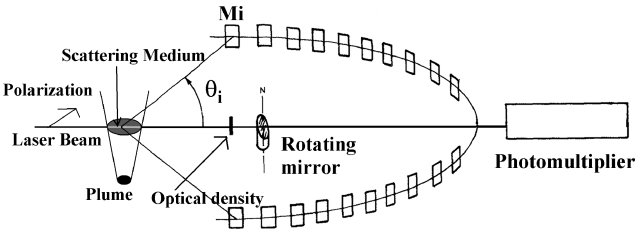

Fig. 2 Nephelometer block diagram (not to scale).

In Situ Light-Scattering Nephelometer

Reference 15 presents a complete and detailed description of the device setup and its associated alignment and calibration procedures. Figure 2 briefly describes the nephelometer used. The plume section is illuminated by a linearly polarized high-power visible laser beam. The scattered light is collected by a set of 20 mirrors M_i placed tangentially along an elliptical path covering scattering angles θ_i from -45 deg to 45 deg. An interferential filter centered on the laser wavelength suppresses any stray light or plume emission at other wavelengths. One focus of this ellipse coincides with the center of the observed volume ΔV defined as the intersection of the laser beam and the field of view (FOV) of the nephelometer here equal to 5 deg. A rotating mirror located at the other focus collects the light sequentially from each mirror M_i. For each scattering angle θ_i, the setup satisfies $\Delta V(\theta_i) \times \Delta\Omega(\theta_i) = \text{const.} \, \forall \theta_i$, where $\Delta V(\theta_i)$ and $\Delta\Omega(\theta_i)$ are respectively the volume observed and the collection solid angle, that is, the full angular aperture $\Delta\theta(\theta_i)$. A photomultiplier tube (PMT) converts the collected light into an electrical signal. We also measure the light transmitted through an optical density to evaluate the optical thickness (OT) for each scattering diagram collected every 20 ms. The scattering diagrams are measured during the experiment's period of stability (in terms of pressure). We only consider the PMT scattering signals that satisfy the OT condition limit: OT ≤ 0.1. The mean and standard deviation (SD) of these signals are then evaluated and corrected using an adequate calibration procedure.

The beam steering effect could provide some difficulties for any particle size measurement technique based on the forward scattering at small angles.[19] In our opinion, the large FOV limits this phenomenon. Moreover, the small variations on the observed volume and its associated mean scattering angle are smoothed by the statistical approach. To consider few residual perturbations, we nevertheless invert the measured data by integrating the theoretical scattering diagrams in the range $[\theta - \Delta\theta, \theta + \Delta\theta]$. Two scattering measurements are performed in plane sections perpendicular to the plume's axis of revolution. Each plume section is characterized by two parameters as described in Table 1: the distance d between the measurement and the nozzle outlet planes and the distance h between the

Table 1 Definition of the different measurements

Measure	d, mm	h, mm	$\varnothing_{\text{plume}}$ estimated, mm
S1	110	0	120
S2	210	85	190

laser beam and the plume axis (see Fig. 1). We investigate the radial variability of PSD in the plume. The scattering data S1 acquired on a diameter of the plume's circular section ($h = 0$) uniformly integrate the contributions of each radial area. The measurement S2 taken on a cord ($h \neq 0$) overestimates the contributions of the external radial zones. By convenience, the measurements S1 and S2 will in the following be referred to as "global" and "external" measurements respectively.

Impact/Collection System

As previous workers,[19–21] we developed and adjusted a subscale SRM to simulate operating conditions similar to those of a full-size engine. Working pressures of about 40 atm and a combustion chamber temperature of approximately 3000°K are obtained. The small quantity of aluminized butalane propellant (2.5 kg) gives a working time of approximately 2 s. Seven experiments were conducted. To not perturb the gas flow and consequently to not interfere with the spectral measurements, the fumes were collected at a distance $L = 4$ m (see Fig. 1) between the impact system and the nozzle outlet plane. We used dry methods to avoid any chemical reactions between the crystalline structures and H_2O as has already occurred in the past.[16] The first experimental setup is an impact system based on a cross-shaped support equipped with retractable pellets holders. The plates made of wood metal are exposed to the plume during 0.2 s. The second setup uses a cyclone technology that is considered efficient in trapping micrometric fumes. A tube is connected to this cyclone and fixed on the cross-shaped impact system. We did not collect the particles close to the nozzle outlet plane. Comparing the parameters issued from the collected powder to those retrieved from in situ optical measurements could be biased. First, the thermal history in the exhaust is very complex, and the collected particles could differ from those locally measured in the plume. Moreover, as the particles are not collected separately according to their size, the presence of aggregates in the collected powder is probable. Because of the distance of collection, we could also point out a potential weaker efficiency of both systems to capture the largest particles, contrary to the small ones that mainly follow the gas.

Analysis of Collected Particles

Morphological Characterization of Collected Al_2O_3 Particles

The collected and impacted particles were characterized by numerous SEM observations. The particles are mainly spherical and range from 0.1 to 20 μm in diameter, the majority being fine particles 0.1 to 2 μm in diameter. The smooth surfaces observed seem to indicate low particle porosity. At a higher magnification, we detected systematic occurrences of large (diameter $\varnothing > 2$ μm) broken hollow spheres (Fig. 3). To verify if small particles could be hollow, TEM observations (Fig. 4) were performed and associated to contrast level measurements as illustrated in Fig. 5. The increase of the contrast in the center of the particle clearly confirms the presence of hollow unbroken small particles. TEM observations also assess that only a few percent of small particles are hollow. The measurement of TEM contrast is limited to small particles ($\varnothing < 2$ μm) where the thickness to be crossed by electron is not too high. We cannot currently confirm if this tendency still occurs in the large size range. In the following, we defined heterogeneity $\varepsilon(R) = R_c/R$ as the ratio of core radius R_c vs the mantle (or total) radius R. SEM and TEM observations are used to evaluate a representative data set of heterogeneity ratios of the observed hollow particles.

Density Estimation and BET Measurements

The powder is collected in the outlet at the bottom of the cyclone. First, a heat treatment at 750°C during 3 h in air is applied to a sample of collected particles to eliminate all of the impurities

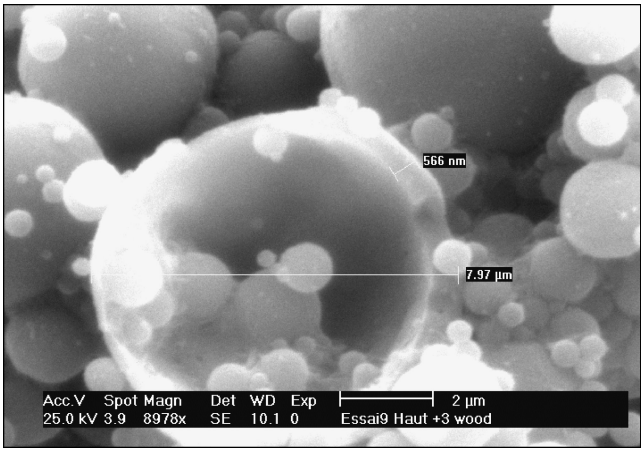

Fig. 3 Broken hollow alumina particle observed by SEM.

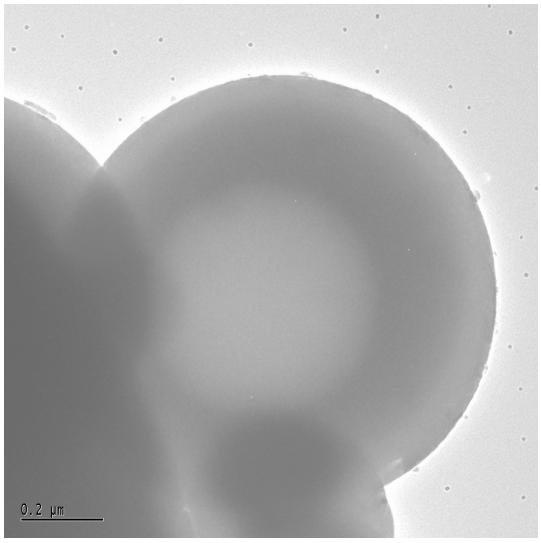

Fig. 4 Hollow alumina particle observed by TEM.

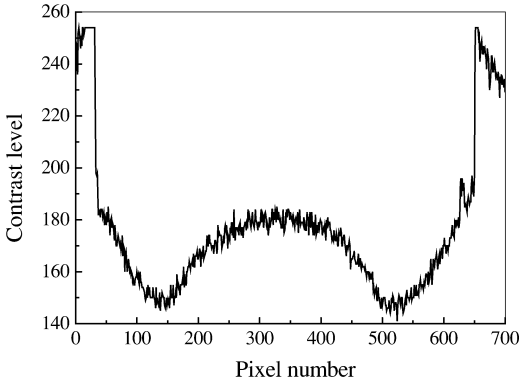

Fig. 5 TEM contrast level diagram.

(2–6% from total weight). Using a helium pycnometer, the measured density obtained on this sample is $\overline{\rho_{\text{meas}}} = 3.55 \pm 0.05$ g/cm^3. Measurements of specific surface area (SSA) can also be used to correlate the mean particle density and the mean particle size and to verify particle porosity. Using BET method on the same sample, the measured SSA is $S_w = 2.56 \pm 0.07$ m^2/g. This low value favors the hypothesis of nonporous particles. The SSA might be related for a distribution of spherical particles to mean particle density $\bar{\rho}$ and mean particle diameter D_{32} through the following relations, for

nonporous [Eq. (1)] and porous [Eq. (2)] spheres, respectively:

$$S_w \approx 6/(D_{32} \times \bar{\rho}) \quad (1)$$

$$S_w \approx 12/(D_{32} \times \bar{\rho}) \quad (2)$$

where the mean particle diameter D_{32} is defined as follows:

$$D_{32} = 2\frac{\int f(R)R^3\,\mathrm{d}R}{\int f(R)R^2\,\mathrm{d}R} \quad (3)$$

where $f(R)$ is the PSD defined by number ($\mu\mathrm{m}^{-4}$). Supposing that the sphere is permeable and using the measured density $\overline{\rho_{\mathrm{meas}}} = 3.55 \pm 0.05$ g/cm^3, we obtain $D_{32} \approx 1.32 \pm 0.06$ μm. According to the SEM analyses, this value overestimates the mean diameter of the particle distribution. This result assesses that the particles are hermetic. As a result, we have $(\bar{\rho} \times D_{32})_{\mathrm{meas}} = 2.35 \pm 0.05$ and $D_{32}^{\mathrm{meas}} = 0.66 \pm 0.03$ μm. This last value will be used in the following sections to assess the data retrieved from PSD measurements.

Empirical Law for Heterogeneous Particles

The existence of large cavities inside the particles is established. Consequently, the presence of hollow spheres needs further explanations. Various processing techniques were developed for making ceramic hollow spheres as a result of their growing potential applications. In particular, rf thermal plasma processing[22] can be used to prepare hollow alumina particles. Thermal plasma ensures high temperature for the particles to melt and is similar in that sense to the SRM operating mode. The phenomena advanced to explain the presence of hollow particles in plasma processing should be considered. A first model was proposed to include the modification of densities between the solid and liquid phases.[23] On cooling, a solid layer grew at the particle surface. Because the density of solid Al_2O_3 $\rho^s_{\mathrm{al_2o_3}}$ is higher than that of liquid Al_2O_3 $\rho^l_{\mathrm{al_2o_3}}$, porosity will form inside the sphere during further solidification. With this assumption, the heterogeneity $\varepsilon = \sqrt[3]{[1 - (\rho^l_{\mathrm{al_2o_3}}/\rho^s_{\mathrm{al_2o_3}})]}$ is independent of the particle radius. As the measured ratios clearly show dependence to the particle radius, this model is inefficient. Another possibility was advanced to explain the presence of hollow spherical ceramic particles.[24] During melting, the release of entrapped gas (in particular water vapor) in the dried agglomerates is supposed to cause the internal cavity.

In SRM, the pressure of gases mainly compounded by H_2, CO, HCl, H_2O, and N_2 is also high (50 atm or more). Liquid alumina is able to dissolve gaseous H_2O, and the spitting effect of liquid alumina under steam atmospheres has already been reported.[25,26] No equivalent Al_2O_3 spitting process exists under other gaseous atmospheres (He, H_2, N_2, O_2, and air).[26] The spitting phenomenon occurs during the liquid to solid transition, which is apparently a very fast reaction. The surplus H_2O is expelled from the Al_2O_3 lattice during the solidification process, mainly near the melting temperature (2327 K) because of the high-speed kinetics involved. To reproduce this spitting phenomenon, an experiment was conducted on a steam aerodynamic levitation device, at atmospheric pressure.[27] After melting a 2-mm-diam alumina droplet with a CO_2 laser, the beam was cut off, and the cooling alumina observed with a high-speed camera (500 Hz). As long as the Al_2O_3 remained liquid, no spitting was observed. However, as soon as the temperature reached the melting point of Al_2O_3, large gas bubbles escaped from the droplet until the alumina became completely solid (Fig. 6). The residue thus obtained was both spherical and hollow.

According to Coutures et al., the total saturation solubility υ_T of H_2O vapor absorbed in the Al_2O_3 lattice is proportional to the square root of the water vapor partial pressure $P^{\mathrm{steam}}_{\mathrm{H_2O}}$ (Ref. 26):

$$\upsilon_T \approx 0.62 \times \sqrt{P^{\mathrm{steam}}_{\mathrm{H_2O}}} + 0.46 \quad (4)$$

For $P^{\mathrm{steam}}_{\mathrm{H_2O}} = 0.83$ atm and pure alumina, they measured $\upsilon_T = 0.97 \pm 0.07$ mg H_2O/g Al_2O_3 and also estimated the saturated solubility contributing to the spitting to be approximately the half of the total saturation solubility: $\upsilon_S = 0.50 \pm 0.05$ mg H_2O/g Al_2O_3. Furthermore, they established that the solubility contributing to spitting υ follows a kinetic process. It increases quickly toward the value of saturation and then decreases more slowly, tending toward an equilibrium value that is around half the saturation value: $\upsilon = 0.25 \pm 0.02$ mg H_2O/g Al_2O_3.

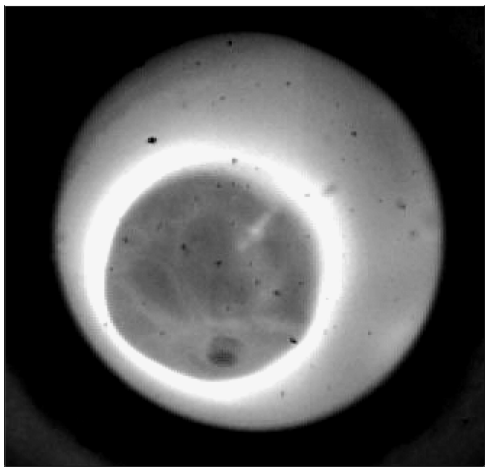

Fig. 6 Alumina droplet under aerodynamic levitation expelling a gas bubble.

Introducing the molar mass $M_{\mathrm{Al_2O_3}} = 0.102$ kg mol^{-1} and density $\rho_{\mathrm{Al_2O_3}} = 2890$ kg/m^3 of liquid alumina,[27] the water steam concentration C^* can be derived as follows:

$$C^* = \frac{\upsilon \times \rho_{\mathrm{Al_2O_3}}}{M_{\mathrm{Al_2O_3}}}\ (\mathrm{mol/m^3}) \quad (5)$$

To understand the occurrence of hollow alumina particles in our collected powder, we applied an empirical model based on a phenomenological approach to spitting. Using the Laplace equations, respectively for a liquid drop in gas and a gaseous drop in liquid, we derived the following relation for a hollow liquid drop:

$$P_i - P_e = 2\sigma(1/R_c + 1/R) \quad (6)$$

where P_i and P_e are the pressures applied on the inner and outer surfaces of the hollow liquid drop, respectively, σ is the surface tension of the liquid material, and R_c and R were already defined. Assuming that H_2O is the only gas dissolved in liquid alumina, the number of gaseous H_2O moles inside the Al_2O_3 spherical particle at the melting point of alumina ($T = 2327$ K) given by the ideal-gas law is

$$n_{\mathrm{H_2O}} = \frac{P_i 4\pi R_c^3}{3\boldsymbol{R}T} \quad (7)$$

In relation (7), the parameter $\boldsymbol{R} = 8.3144$ J mol^{-1} K^{-1} is the universal gas constant. The solubility υ of H_2O in liquid Al_2O_3 contributing to spitting can be expressed as

$$\upsilon = \frac{n_{\mathrm{H_2O}}}{n_{\mathrm{Al_2O_3}}} = \frac{M_{\mathrm{Al_2O_3}} P_i R_c^3}{\rho_{\mathrm{Al_2O_3}} \boldsymbol{R}T\left(R^3 - R_c^3\right)} \quad (8)$$

and consequently, the water steam concentration C^* is

$$C^* = \frac{P_i R_c^3}{\boldsymbol{R}T\left(R^3 - R_c^3\right)}\ (\mathrm{mol/m^3}) \quad (9)$$

Identifying the P_i expressions in relations (9) and (6), we finally derived a formulation that relates the radius to the heterogeneity ε and the concentration C^*:

$$R = g(\varepsilon, C^*) \quad (10)$$

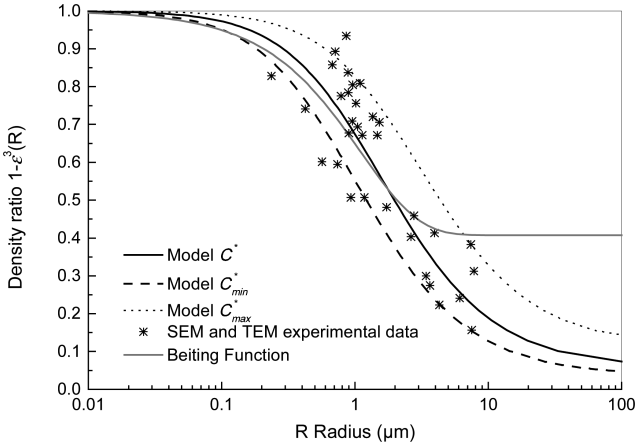

Fig. 7 Comparison of relative density ratios.

where

$$g(\varepsilon, C^*) = \left[\frac{(2\sigma/C^*\boldsymbol{R}T) \times (\varepsilon^2 + \varepsilon^3)}{1 - \left[(1 + P_e/C^*\boldsymbol{R}T) \times \varepsilon^3\right]}\right] \tag{11}$$

In relation (11), the external pressure value and surface tension of liquid alumina at the melting point were respectively set at the following values: $P_e = 10^5$ Pa, and $\sigma = 0.65$ N/m (Ref. 27). SEM and TEM observations gave a data set of heterogeneity ratios $\varepsilon(R) = R_c/R$ that is relatively dispersed. We first derived the smooth concentration C_f^* fitting these ratios. A simple iterative method on the concentration C^* is used to minimize the following function:

$$F = \frac{1}{N}\sum_{i=1}^{N}\left[\frac{R_i - g(\varepsilon_i, C^*)}{R_i}\right]^2 \tag{12}$$

where R_i and ε_i are respectively the measured radius and the corresponding measured heterogeneity ratio and N the number of data. We obtained $C_f^* \approx 85$ mol/m^3. Identifying for each radius R the relation (10) and using a simple iterative method on the heterogeneity, its corresponding law of heterogeneity $\varepsilon(R, C_f^*)$ was then derived. Applying this method, we also constructed two bounding functions $\varepsilon(R, C_f^* \pm \Delta C^*)$. We increased the parameter ΔC^* until these limit functions defined an interval including 90% of the experimental points (see Fig. 7). We obtained $\Delta C^* = 45$ mol/m^3, that is, $C_{\min}^* \approx 40$ mol/m^3 and $C_{\max}^* \approx 130$ mol/m^3. To improve our approach, we compared our semi-empirical approach to a fitting model of density published in the work of Beiting.[17] It expresses the individual density ratio (density of bulk alumina $\rho_{\text{bulk}} = 3.97$) of a particle as a function of diameter as follows:

$$\rho(R)/\rho_{\text{bulk}} = 0.416 + 0.605 \times 10^{-0.39R} \tag{13}$$

This empirical model was derived to fit the retrieved densities of the small particles observed in stratospheric exhausts of large SRM. This model only considered small particles less than 5 μm as larger ones are not captured because of sedimentation effect. In Fig. 7, we confront this model with our own empirical model according to $\rho(D)/\rho_{\text{bulk}} = 1 - [\varepsilon(R, C^*)]^3$. The Beiting model and our models give an identical behavior for particles below 5 μm in diameter.

Particle Sizing

Theoretical Background

Noisy inverse problems are "ill conditioned" and have endless solutions. So, both the accuracy and stability of the resulting distribution function from noisy data are generally poor and require regularization. We developed a specific inverse method where regularization is based on a numerical filtering approach that is self-consistent with data uncertainties (see Refs. 14 and 15 for more details). The measured media are made of randomly distributed spheres with a known law of heterogeneity $\varepsilon(R)$. These media are illuminated by a linearly polarized laser at wavelength λ_0 or a spectral source in the range $[\lambda_{\min}, \lambda_{\max}]$. The relative refractive index at wavelength λ of the core and the mantle are $m_c(\lambda)$ and $m_m(\lambda)$, respectively. Using adequate experimental setups, mean scattering signals at scattering angle θ_i, and mean spectral data at wavelength λ_i (defined in the surrounding media) are respectively proportional to the integrated differential scattering cross section $S(\theta_i)$ and the extinction coefficient $K_e(\lambda_i)$, which are defined by

$$S(\theta_i) = \int_0^\infty f(R)\int_{\theta_i - \Delta\theta_i}^{\theta_i + \Delta\theta_i} \frac{\mathrm{d}C_s}{\mathrm{d}\Omega}\left[\frac{R}{\lambda_0}, m_c(\lambda_0), m_m(\lambda_0), \varepsilon(R), \theta\right]\mathrm{d}\theta\,\mathrm{d}R \tag{14a}$$

$$K_e(\lambda_i) = \int_0^\infty f(R)C_e\left[\frac{R}{\lambda_i}, m_c(\lambda_i), m_m(\lambda_i), \varepsilon(R)\right]\mathrm{d}R \tag{14b}$$

In the preceding relations, $\mathrm{d}C_s/\mathrm{d}\Omega$ is the differential scattering cross section for a linearly polarized laser, and C_e is the extinction cross section, both evaluated using an algorithm based on the work of Toon and Ackerman.[28] Equations (14) are written in a more general form:

$$U(x_i) = \int_0^\infty f(R)\psi(R, x_i)\,\mathrm{d}R \tag{15}$$

where U is proportional to the measured data and x_i is a discrete parameter of the measurement and assuming N discrete measurements. A system of N Fredholm integral equations of the first kind was then defined and transformed as follows:

$$U(x_i) = \int_{R_{\min}}^{R_{\max}} h(R)\Gamma_{x_i}(R)\,\mathrm{d}R \tag{16}$$

with

$$\Gamma_{x_i}(R) = \frac{\psi(R, x_i)\exp(-\gamma R)}{\pi R^2} \tag{17}$$

$$h(R) = \pi R^2 \exp(\gamma R) f(R) \tag{18}$$

Parameters γ and $R_{\min}$ were evaluated by the program and depend on the value of $R_{\max}$ supplied by the user. At step p of the numerical filtering scheme, the function $h(R)$ was written as the sum of $M(p) \le N$ cubic B-spline functions $S_j^p(R)$, having nodes defined by cutoff frequency $\omega_{\max}(p-1)$. This frequency results from the numerical filtering process and evaluated using distribution $h^{p-1}(R)$ and data uncertainties $\Delta U(x_i)$ (see Ref. 14 for more details). By setting the spline decomposition in the relation (16), an overdetermined linear system is obtained and solved[29] to give the spline decomposition coefficients c_j^p. The global iterative algorithm is performed, although the stopping criterion $|\omega_{\max}(p) - \omega_{\max}(p-1)| < \varepsilon_\omega$ is not verified. When the method achieves global convergence, the best linear approximation of distribution function $h^\infty(R)$ is obtained and finally yields the smooth PSD $f^\infty(R)$. In the following, the solution is expressed by volume according to

$$v(R) = f^\infty(R) \times V_p(R) \tag{19}$$

where $V_p(R) = 4\pi R^3/3$ and is normalized for the graphical representation using the relation:

$$v(R) = v(R)/\max_R[v(R)] \tag{20}$$

Parameters Retrieved from PSD

Physicochemical characterizations[7–9] indicate that 20–40% of the powder mass is made of α-Al_2O_3. The remaining 60–80% is a complex spinel-type compound denoted γ-Al_2O_3. Using micro-Raman microscopy, we have also observed that the smaller drops less than 3 μm in diameter do not contain α-Al_2O_3. Using the smooth PSD, we derived few physical parameters and compared them to the equivalent data from the physicochemical particle analyses: the mean diameter D_{32} [see Eq. (3)], the mean density $\bar{\rho}$, and

the mass fraction of spinel phases η. Each phase has its own density: $\rho_\alpha = 3.97$ g/cm^3 and $\rho_\gamma = 3.65$ g/cm^3. The density of alumina $\rho(R)$ is thus a function of the radius:

$$\rho(R) = \rho_\gamma \quad \forall R < R_L \qquad \rho(R) = \rho_\alpha \quad \forall R > R_L \tag{21}$$

The mean density $\bar{\rho} = f_m / f_v$ is the ratio between the volume mass f_m (in g/cm^3) and the volume fraction f_v, respectively, defined by

$$f_m = \int f(R) V_p(R) \varsigma(R) \rho(R)\, \mathrm{d}R \tag{22}$$

$$f_v = \int f(R) V_p(R)\, \mathrm{d}R \tag{23}$$

where $\varsigma(R) = 1 - \varepsilon(R)^3$. Physicochemical analyses also give the ratio η of the mass of the γ spinel phases to total mass. Using the retrieved PSD, this ratio is calculated as follows:

$$\eta = f_m^\gamma \Big/ f_m \tag{24}$$

with

$$f_m^\gamma = \int_{R_{\min}}^{R_L} f(R) V_p(R) \varsigma(R) \rho_\gamma\, \mathrm{d}R \tag{25}$$

Results

PSD by Inversion of Scattering Data

The shots experiments have a very brief stability period of around 1.3 s. Only $P = 50$ scatter diagrams consisting of 20 discrete scattering angles and P transmission measurements were performed. The mean diagrams and their confidence intervals for the two measurements are presented in Fig. 8.

Because of the relatively small number P of scattering diagrams and plume instability, large uncertainties are observed. The associated noise levels are around 17% for the global measurement and around 30% for the external one. Because of turbulence phenomena, plume stability decreases as the distance to the plume center increases. External scattering data consequently present a higher noise level than global ones.

The measurements are performed between the nozzle outlet plane and the first recompression zone (Mach disks). Because of the high cooling rate of the particles, a phase transition liquid to solid could occur in this area and the probability to have hollow particles exists. Consequently, we invert the scattering diagrams considering that all of the observed particles are hollow or full. The Anfimov model[30] is used to predict the evolution of optical indices of Al_2O_3 at a high temperature, here set at 1800 K following aerothermochemical simulations performed to evaluate the temperature of the particles for the subscale SRM used. The retrieved normalized smooth PSD $v(R)$ obtained for each scattering diagram is presented in the following

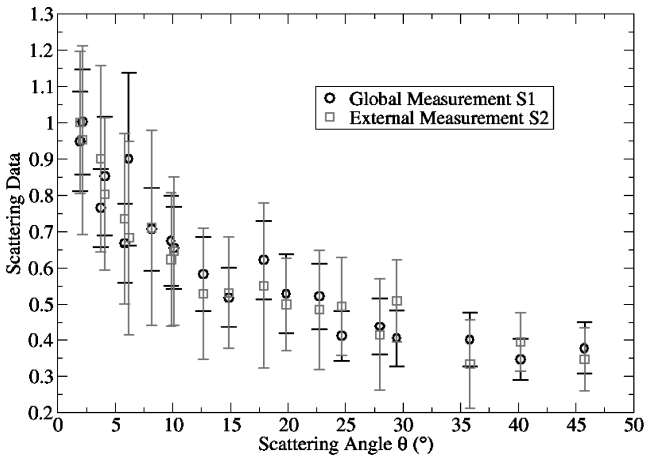

Fig. 8 Scattering data for the shots.

Table 2 Retrieved parameters for both in situ measurements

Data	D_{32}^{hom}	$\overline{\rho_{\text{hom}}}$	η_{hom}	D_{32}^{het}	$\overline{\rho_{\text{het}}}$	η_{het}
S1	0.42	3.7	0.87	0.65 ± 0.10	2.20 ± 0.50	0.84 ± 0.04
S2	0.49	3.7	0.89	0.43 ± 0.05	2.95 ± 0.25	0.94 ± 0.02

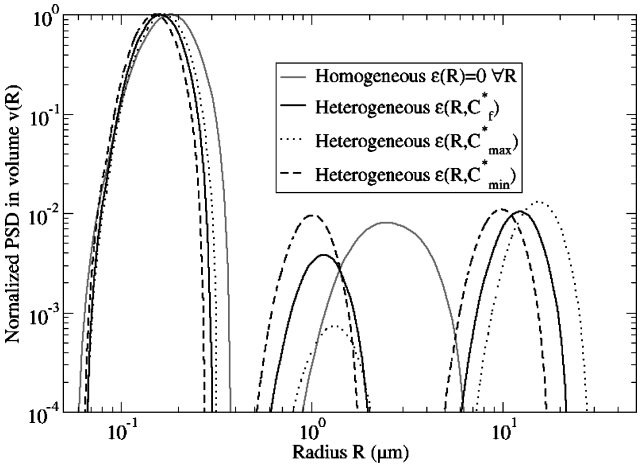

Fig. 9 Normalized smooth PSD $v(R)$ for S1.

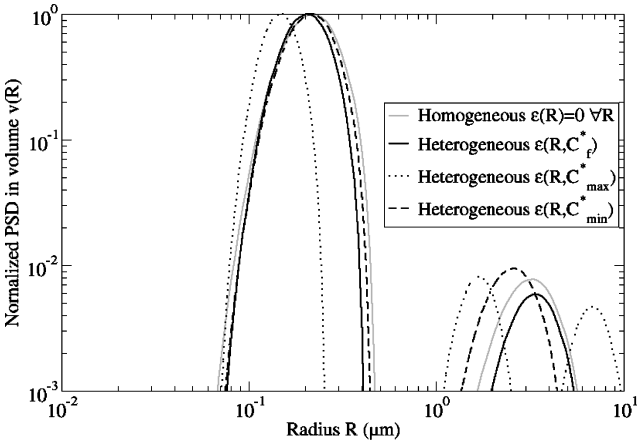

Fig. 10 Normalized smooth PSD $v(R)$ for S2.

figures. For global data (see Fig. 9), the assumption of homogeneous spheres gives a bimodal PSD. The two wide peaks are respectively centered near 0.2 and 2.5 μm. Using the three heterogeneity laws, a trimodal distribution is obtained. A peak of larger particles centered near 12 μm appears. The second mode is translated to a smaller median radius near 1.25 μm and is narrower. The first peak is also subject to a minor translation toward small radii and is located near 0.15 μm. For the external data set, the retrieved PSDs are less influenced by particle heterogeneity, even if differences still remain on the localization of both peaks (see Fig. 10). It can be considered that the high noise level reduces the sensitivity of the inverse method. Only the more heterogeneous assumption obtained with the value $C^*_{\max}$ gives trimodal distribution.

We used the PSD $v(R)$ and associated heterogeneity law $\varepsilon_{\text{het}}(R)$ defined in the preceding section to evaluate the mean diameter, the mean density range, and the mass fraction of the gamma phase. In Table 2, we compare the parameters of the global and external measurements.

Suppose that heterogeneous spheres give a global D_{32} larger than the external one, whereas this tendency is inverted if we assume that the spheres are full. Aerothermochemical simulations of the plume show that the heavier particles remain concentrated in the center of the plume, whereas the lighter particles are uniformly distributed throughout the plume because they follow the combustion

gases. Therefore, the PSD obtained in the external radial layers of the plume must have a lower mean radius than a PSD including all of the concentric layers. From this point of view, the results obtained assuming heterogeneity are more accurate. We now confront the global parameters obtained using the heterogeneous and homogeneous assumptions with the parameters directly estimated from the analyses of the collected particles, that is, $\eta_{\text{meas}} \cong 0.7 \pm 0.1$, $D_{32}^{\text{meas}} = 0.66 \pm 0.03$, and $\overline{\rho_{\text{meas}}} = 3.55 \pm 0.05$. The retrieved heterogeneous in situ mean diameter $D_{32}^{\text{het}} = 0.65 \pm 0.1$ is close the estimated value on the collected powder $D_{32}^{\text{meas}} = 0.66 \pm 0.03$, whereas homogeneous assumption gives a lower value. The in situ gamma mass fraction and mean density respectively overestimates and underestimates the values obtained on the collected powder.

PSD by Inversion of Extinction Data

A 1% in mass Al_2O_3-KBr mixture was prepared and then pressed to form two pellets. The spectral transmittances of these pellets and of a KBr reference pellet were measured using a Fourier transform infrared spectrophotometer from 370 to 7500 cm^{-1}. The results are presented in Fig. 11. Both pellets give similar transmittances. To derive spectral data to be inverted, we first verify that pellet thickness is constant. The residual porosity of KBr is also assumed to remain identical for all of the samples. With these assumptions, the spectral data $\beta(\varpi)$ proportional to the extinction coefficient are derived according to

$$\beta(\varpi) = cste \times \ln[t_{\text{sample}}(\varpi)/t_{\text{KBr}}(\varpi)] \tag{26}$$

We first interpolate the spectral data $\beta(\varpi)$ in a finite set of $N = 31$ wavelengths $[\lambda_i]$ that are equally spaced in the spectral range [2–12 μm]. We then calculate the mean of $\beta(\lambda)$ obtained on the two pellets, and we define random uncertainties having a mean SD set at 20% in order to compare the PSD retrieved from extinction data to those issued from scattering measurements. The corresponding data are presented in Fig. 12.

The inversion of extinction data requires an a priori knowledge of the optical indices of alumina and KBr, which are obtained from bibliographical data.[31] The noisy extinction data are inverted with the assumption of homogenous spheres. The resulting normalized smooth PSD $v(R)$ in volume is presented in Fig. 13. Residual aggregates of individual particles give a fourth mode located near 50 μm. Eliminating this mode, we evaluate the parameters corresponding to this PSD and compare them to the measured ones (see Table 3).

Table 3 Powder parameters

Data type	D_{32}	$\bar{\rho}$	η
Measured	0.65 ± 0.10	3.55 ± 0.05	0.7 ± 0.1
Evaluated	0.56	3.74	0.74

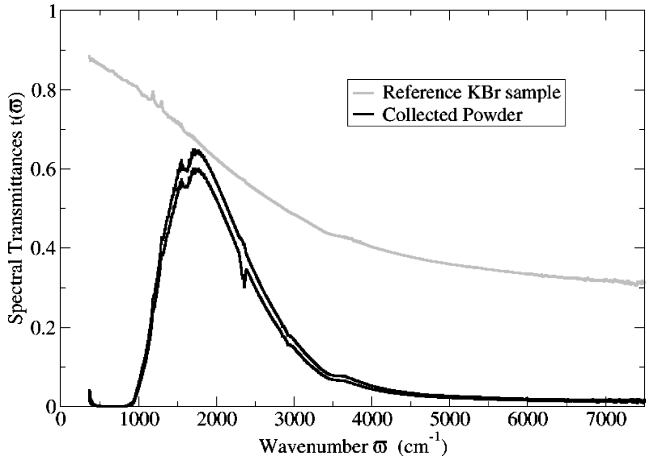

Fig. 11 Measured spectral transmittances.

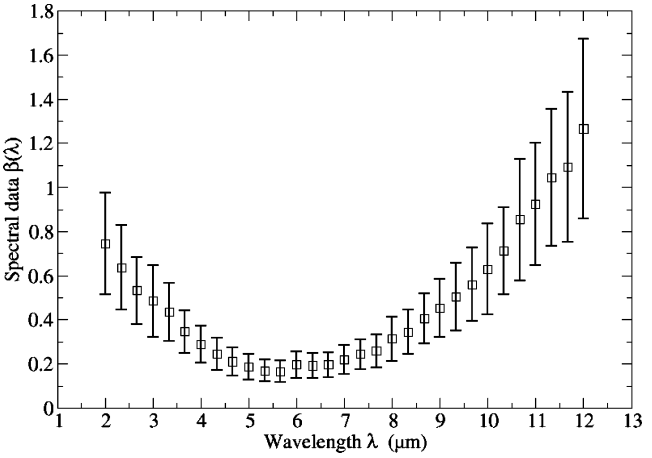

Fig. 12 Mean and SD of $\beta(\lambda)$ for the powder.

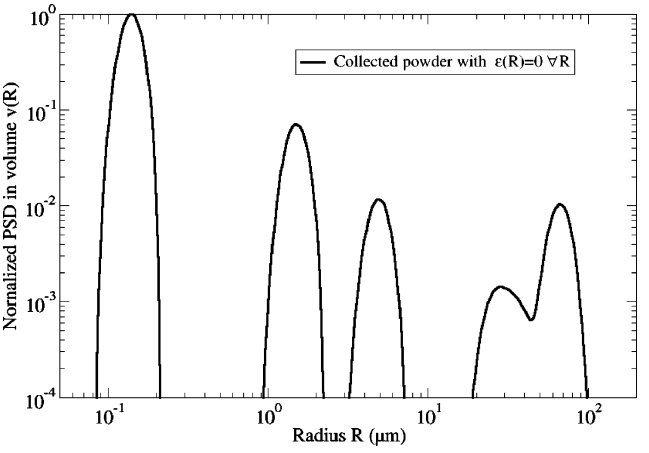

Fig. 13 Normalized smooth PSD $v(R)$ for powder.

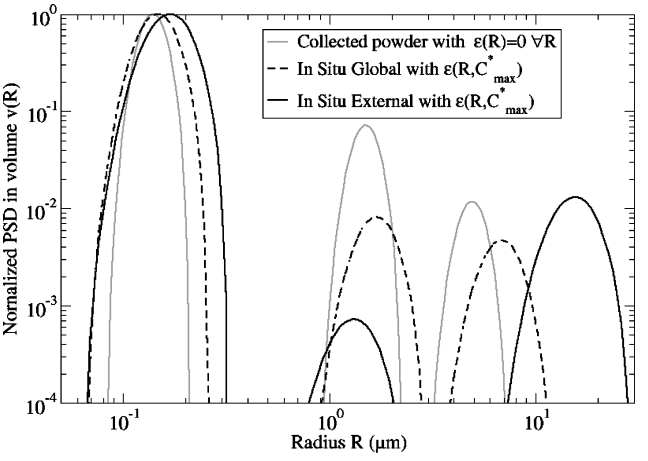

Fig. 14 Normalized smooth PSD $v(R)$ for powder and in situ measurement.

Considering the uncertainties, the data are close. The underestimation of the evaluated mean diameter can be related to the presence of aggregates in the powder. In the physicochemical analyses of density and gamma mass fraction, the aggregates do not interfere. The lack of density can be explained as the powder contains a small fraction of hollow particles. In Fig. 14, we confront the PSD of the powder to the in situ measured ones. The small particles present identical modes. This result tends to infirm the lack of efficiency of the cyclone to collect large particles as already mentioned. The modes are weakly shifted toward smaller radii. This phenomenon

seems to be more intense for large particles. An explanation can be tentatively proposed. A hollow particle crosses all of the recompression (Mach disks) and postcombustion zones that could present very high temperatures over the melting point. If we consider a weak thermal inertia, this particle could melt. The residual water steam in this new liquid particle could be then insufficient to induce a novel spitting. A full sphere with a lower radius satisfying the mass conservation is finally obtained. This phenomenon could also explain the small fraction of hollow particles in the collected powder.

Discussion

Water Steam Concentration

We have plausibly suggested that there is spitting at the liquid to solid transition, which would explain the heterogeneity of collected particles. Therefore, we assumed the water steam concentration before solidification to be unknown. We proposed a simple empirical model to predict particle heterogeneity using this value as an adaptable fitting parameter. Using experimental techniques to determine the heterogeneity directly from powder analysis, we estimate the water steam concentration $C^* = 85 \pm 45$ mol/m^3 fitting the experimental values. Coutures et al. have experimentally studied the spitting of water steam in alumina. Even if the SRM operating conditions are far from the working characteristics of their experiments, it could be of interest to discuss how the work of Coutures et al. could corroborate our estimation of the water steam concentration. The incorporation of steam water in an alumina liquid droplet is a kinetic process. As a consequence, it mainly depends on the temperature, size of the liquid droplet (i.e., the surface exchange), and melting time. In a SRM chamber, gases and liquid alumina drops reach a temperature of nearly 3000 K. The size of liquid alumina droplets is typically between 20 and 200 μm before breakup, and their lifetime can be estimated between a few milliseconds and a few tens of milliseconds. Deriving a kinetic law predicting the steam water's concentration as a function of time for those liquid droplets at very high temperature is difficult. Nevertheless, we can reasonably presume that the maximum or equilibrium values and their relative ratios are globally unchanged. Considering this hypothesis and also supposing that the relation (4) is conserved for $P_{H_2O}^{steam} = 5$ atm, the concentration contributing to spitting should lie within the 120 ± 50 mol/m^3 range that is relatively close to our results. Additionally, in the SRM shot a complex mixture made of α-Al_2O_3 and spinel-type alumina denoted γ-Al_2O_3 is formed,[7–9] whereas in Coutures work, we can anticipate pure α-Al_2O_3. As the difference of density between liquid and solid states for γ-Al_2O_3 decreases, the concentration contributing to spitting for a SRM exhaust mainly made of γ-Al_2O_3 could be reduced and can contribute to moderate the retrieved concentration on the collected particles.

How Could the Results Be Representative of a Full-Size SRM?

The presented results have been obtained on a subscale SRM. Such experiments have been intensively used to study the alumina particles[19–21] exhaust or the validation of stability prediction[32] in SRM. As already mentioned, the SRM used in this paper was specially developed to deliver a specific set of representative operating conditions of a full-size SRM. Nonetheless, we could wonder if the behaviors described in this paper could be also present in a full-size SRM. It is impossible to answer to this question in an absolute way because many factors should be considered. Nevertheless, few arguments could be underlined in favor of discussing this question.

As the spitting could interact concurrently with the breakup and coalescence event, a most recent campaign of shots experiments has been performed on the same subscale SRM used in this work. An identical AP-HTPB-Al propellant was burned, but the nozzle was less divergent. Higher working pressures of about 50 atm were also obtained. The collected particles verify the heterogeneous laws presented in this paper. Using the heterogeneous laws described here and assuming all of the particles are hollow, quite identical PSD were retrieved. These results seem to indicate a moderate influence of nozzle geometry on the spitting phenomenon. Nevertheless, the fraction of hollow particles is reduced and becomes less than 1%. This tendency is confirmed by the measurement of mean density: $\bar{\rho}_{meas} = 3.80 \pm 0.04$. In this second campaign, higher temperatures of the particles and the gases were revealed by the IR observations. We can reasonably suppose that the probability for a hollow particle to melt before its capture was enforced.

We could also point out previous observations of hollow particles for various subscale SRM associated with the Aerodynamics of Segmented Solid Motors program,[32] which was devoted to characterize the Ariane V SRM. Different operating conditions and AP-HTPB-Al propellants were used to perform many shots. Very large hollow particles were observed during these shots. Unfortunately, this point was not further investigated.

Another statement could be mentioned in order to support the potential applicability of our results for full-size SRM. We can notice that the in situ mean density derived in this paper is close to the density 2.5 ± 1 g/cm^3 range reported in previous work.[5,17] This value was obtained on full-size SRM at high altitudes having PSD close to ours. As high altitudes considerably reduce the plume temperature, the consequences of the spitting phenomenon could be then less affected by the thermal structure of the plume.

Conclusions

The morphological properties of alumina particles collected during subscale SRM tests are fully characterized. The characterization of these powders by TEM and SEM indicates that drops are formed from spherical particles between 0.1 and 20 μm in diameter. These drops could be hollow, and, in view of the BET results, the particles are probably nonporous. The formation of hollow particles is then justified by the spitting phenomenon that occurs during the solidification process and is caused by the presence of gaseous H_2O inside the combustion chamber. Despite the complexity of describing the spitting phenomenon in a SRM, an empirical predictive model is introduced. Its validity and its accuracy are widely discussed.

Particle size analysis based on two inverse methods associated with appropriate experimental setups is carried out. These methods are based on in situ light scattering measurements or the spectral extinction characterization of collected particles. Integrating an empirical model predicting heterogeneity into inverse method fits the retrieved in situ PSD well from an aerothermochemical point of view, thus backing up the pertinence of the empirical heterogeneity law. Using reasonable assumptions on the collected particles, the comparison of in situ PSDs and those derived from extinction data on collected particles is consistent. Furthermore, considering all of the uncertainties, the parameters retrieved from the PSD of collected particles are reasonably close to the equivalent measured data.

A recent campaign confirms the heterogeneous laws to be pertinent but clearly shows that the fraction of the hollow particles in the collected powder is variable. This result points out the complex evolution of the morphology and PSD in the plume. For a better comprehension of these evolutions, we intend to perform systematic morphological size and physicochemical characterization of particles collected in different zones of large SRM using a more efficient collection system based on a 13-levels cascade impactor. New optical in situ granulometers under development would be also used to perform local analyze of dense scattering media.

Acknowledgments

The research reported herein was performed in collaboration with the Centre de Recherche sur les Matériaux à Haute Température (CRMHT), Orléans, France. The authors wish to acknowledge Francis Millot of the CRMHT for his contribution in the analysis of the results. We also acknowledge Emmanuel Veron of the CRMHT and Carolinne Andreazza of the Centre de Recherche sur la Matière Divisée, Orléans, France, who have performed the scanning-electron-microscopy/transmission-electron-microscopy characterizations.

References

[1]Roblin, A., Dubois, I., Grisch, F., Boischot, A., and Vingert, L., "Comparison Between Computations and Measurements of a H2/LOX Rocket Motor's Plume," AIAA Paper 2002-3107, June 2002.

[2]Baudoux, P. E., Chervet, P., and Roblin, A., "A New Approach for Radiative Transfer Computations in Axisymmetric Scattering Hot Media," *Journal of Thermophysics and Heat Transfer*, Vol. 15, No. 3, 2001, pp. 317–325.

[3]Roze, P., Henry, D., and Langlois, S., "PRF-SIRJET. Dépouillement des Mesures Infrarouges Réalisées au Banc LP11 du CFM en Janvier-Fevrier 2002," ONERA, Rept. RT 4/07041 DOTA, Palaiseau, France, Jan. 2003.

[4]Murphy, P. J., and Reed, R. A., "Measurement and Analysis of Laser Transmission Through Solid-Propellant Rocket Motor Exhaust Plumes," AIAA Paper 93-2886, July 1993.

[5]Strand, L. D., Bowyer, J. M., Varsi, G., Laue, E. G., and Gauldin, R., "Characterization of Particulates in the Exhaust Plume of Large Solid-Propellant Rockets," *Journal of Spacecraft and Rockets*, Vol. 18, No. 4, 1981, pp. 297–305.

[6]Rodionov, A. V., Plastinin, Y. A., Drakes, J. A., Simmons, M. A., and Hiers, R. S., "Modeling of Multiphase Alumina-Loaded Jet Flow Fields," AIAA Paper 98-34623, July 1998.

[7]Gossé, S., "Caractérisations Morphologiques et Radiatives des Alumines Issues de la Combustion de Propergol. Application au Transfert Radiatif dans les Jets," Ph.D. Dissertation, Orléans Univ., France, Jan. 2004.

[8]Gossart, P., "PRF SIRJET de Missiles Supersoniques—Campagne de Tirs au Fauga-Mauzac. Rapport sur les Différentes Analyses Physico-Chimiques et Morphologiques de Particules," ONERA, Technical Rept. RT 4/08373 DOTA, Palaiseau, France, April 2004.

[9]Gossé, S., Sarou-Kanian, V., Véron, E., Millot, F., Rifflet, J. C., and Simon, P., "Characterization and Morphology of Particles in Solid Propellant Subscale Rocket Motors," AIAA Paper 2003-3649, June 2003.

[10]Hespel, L., Delfour, A., Gossé, S., and Millot, F., "Influence of Alumina Particles Heterogeneity on Particle Sizing and Radiative Properties Evaluation in Solid Rocket Plumes," AIAA Paper 2003-3650, June 2003.

[11]Jones, M. R., Curry, B. P., Brewster, M. Q., and Long, K. H., "Inversion of Light Scattering Measurement for Particle Size and Optical Constants: Theoretical Study," *Applied Optics*, Vol. 33, No. 18, 1994, pp. 4025–4034.

[12]Jones, M. R., Long, K. H., Brewster, M. Q., and Curry, B. P., "Inversion of Light Scattering Measurement for Particle Size and Optical Constants: Experimental Study," *Applied Optics*, Vol. 33, No. 18, 1994, pp. 4035–4041.

[13]Jones, M. R., Brewster, M. Q., and Yamada, Y., "Application of a Genetic Algorithm to the Optical Characterization of Propellant Smoke," *Journal of Thermophysics and Heat Transfer*, Vol. 2, No. 2, 1996, pp. 372–377.

[14]Hespel, L., and Delfour, A., "Mie Light-Scattering Granulometer with Adaptive Numerical Filtering. I. Theory," *Applied Optics*, Vol. 39, No. 36, 2000, pp. 6897–6917.

[15]Hespel, L., Delfour, A., and Guillame, B., "Mie Light-Scattering Granulometer with Adaptive Numerical Filtering. II. Experiments," *Applied Optics*, Vol. 40, No. 6, 2001, pp. 974–985.

[16]Salita, M., "Survey of Recent Al_2O_3 Droplet Size Data in Solid Rocket Chambers, Nozzles, and Plumes," *31st JANNAF Combustion Meeting*, Oct. 1994.

[17]Beiting, E. J., "Solid Rocket Motor Exhaust Model for Alumina Particles in the Stratosphere," *Journal of Spacecraft and Rockets*, Vol. 34, No. 3, 1997, pp. 303–310.

[18]Von Wartenberg, H., "Wasserabsorption Durch Schmelzende Oxyde," *Zeitschrift für Anorganische und Allgemeine Chemie*, Vol. 264, No. 5–6, 1951, pp. 226–229.

[19]Laredo, D., McCrorie, J. D., II, Vaughn, J. K., and Netzer, D. W., "Motor and Plume Particle Size Measurement in Solid Propellant Micromotors," *Journal of Propulsion and Power*, Vol. 10, No. 3, 1994, pp. 410–418.

[20]Kim, H.-O., Laredo, D., and Netzer, D. W., "Measurement of Submicrometer Al_2O_3 Particles in Plumes," *Applied Optics*, Vol. 32, No. 33, 1993, pp. 6834–6840.

[21]Brennan, W. D., Hovland, D. L., and Netzer, D. W., "Measured Particulate Behavior in a Subscale Solid Propellant Rocket Motor," *Journal of Propulsion and Power*, Vol. 8, No. 5, 1992, pp. 954–960.

[22]Karoly, Z., and Szépvölgyi, J., "Hollow Alumina Microspheres Prepared by RF Thermal Plasma," *Powder Technology*, Vol. 132, No. 2–3, 2003, pp. 211–215.

[23]Klima, R., and Kotalik, P., "On Cavities in Thermally Spheroidized Powder Particles," *Journal of Thermal Spray Technology*, Vol. 6, No. 3, 1997, pp. 305–308.

[24]Pravdic, G., and Gani, M. S. J., "Formation of Hollow Spherical Ceramic Oxide Particles in a d.c. Plasma," *Journal of Materials Science*, Vol. 31, No. 13, 1996, pp. 3487–3495.

[25]Diamond, J. J., and Dragoo, A. L., "Studies of Molten Alumina in the Arc-Image Furnace," *Revue des Hautes Températures et des Réfractaires*, Vol. 3, 1966, pp. 273–279.

[26]Coutures, J. P., Devauchelle, J. M., Munoz, R., and Urbain G., "Dissolution of Water Vapor in SiO_2-Al_2O_3 Melts," *Revue Internationale des Hautes Températures et des Réfractaires*, Vol. 17, 1980, pp. 351–361.

[27]Millot, F., Glorieux, B., and Rifflet, J. C., "Measurements of the Physico-Chemical Properties of Liquid Alumina Using Contactless Techniques," *Solid Propellant Chemistry, Combustion, and Motor Interior Ballistics*, edited by V. Yang, T. B. Brill, and W.-Z. Ren, Progress in Astronautics and Aeronautics, Vol. 185, AIAA, Reston, VA, 2000, pp. 777–788.

[28]Toon, O. B., and Ackerman, T. P., "Algorithms for the Calculation of Stratified Spheres," *Applied Optics*, Vol. 20, No. 20, 1981, pp. 3657–3661.

[29]Lawson, C. L., and Hanson, R. J., "Linear Least Squares with Linear Inequality Constraints," *Solving Least Squares Problems*, Series in Automatic Computation, Prentice–Hall, Englewood Cliffs, NJ, 1974, pp. 158–173.

[30]Anfimov, N. A., Karabadjak, G. F., Khmelinin, B. A., Plastinin, Y. A., and Rodionov, A. V., "Analysis of Mechanisms and Nature of Radiation of Aluminum Oxide in Different Phase States in Solid Rocket Exhaust Plumes," AIAA Paper 93-2818, July 1993.

[31]Palik, E. D., *Handbook of Optical Constants of Solids II*, Academic Press, San Diego, CA, 1991, pp. 989–1004.

[32]Prevost, M., Godon, J. C., and Maunoury, J., "Overview on the Representativity of Small Scale Motor Tests," ONERA, Rept. TPND 2005-1 DMAE, Le Fauga-Mauzac, France, 2005.